First-principles study of the high-pressure suppression of magnetic moments in $CeIn_3$

Mansoure Ilkhani,[1,*] Mohammad Reza Abolhassani,[2,3] and Morteza Aslaninejad[2]
[1]*Shahr_e_Qods-Shahryar, Islamic Azad University, P.O. Box 37515–374, Shahr_e_Qods, Iran*
[2]*Plasma Physics Research Center, Science and Research Branch, Islamic Azad University, P.O. Box 14665-67, Tehran, Iran*
[3]*Department of Physics, Tarbiat Modares University, P.O. Box 14115-111, Tehran, Iran*
(Received 26 October 2008; revised manuscript received 22 August 2009; published 30 September 2009)

We use the first-principles full-potential augmented plane-wave plus local-orbital methods to calculate the electronic structure and hyperfine electric interaction of antiferromagnetic $CeIn_3$ compound. In addition to the Perdew-Burke-Ernzerhof (PBE) generalized gradient approximation, a more accurate nonempirical density-functional Wu-Cohen generalized gradient approximation (GGA) for the exchange-correlation energy is implemented in the calculations. Results show an almost linear fall of spin magnetic moments of Ce by increasing the pressure. Cerium f states move away from the Fermi level into the conduction band by imposing the pressure which causes the suppression of the magnetic moment in the vicinity of a critical pressure around 9 GPa. A bow shape increase in electric field gradient at In sites is observed under pressure. While Wu and Cohen-GGA approach leads to a good agreement between the critical pressure and bulk modulus values and their experimental data at ambient pressure, it does not amend the values of the lattice constant and electric field gradient of $CeIn_3$, calculated through the standard PBE-GGA.

DOI: 10.1103/PhysRevB.80.125131 PACS number(s): 71.20.−b, 71.27.+a, 31.30.Gs, 75.20.Hr

I. INTRODUCTION

The intermetallic compound $CeIn_3$ is an interesting system composed of strongly correlated $4f$ electrons. It is a Kondo system with a heavy fermion behavior at low temperatures.[1] It shows unexpected physical properties,[2] originating from the fact that one cannot assign a specific localization to the $4f$ states without considering the conditions imposed on the $CeIn_3$. This unexpected physical behavior may be then attributed to the degree of localization of the $4f$ electrons, i.e., the position of the $4f$ density of states ($4f$-DOS) with respect to the Fermi level. The position of the $4f$-DOS demonstrates the degree of hybridization between localized $4f$ and conduction bands. It also undergoes an antiferromagnetic (AFM) order below Néel temperature $T_N = 10$ K with an ordered moment of $0.65 \pm 0.1 \mu_B$ per Ce atom at ambient pressure.[2] There is a competition between Ruderman-Kittel-Kasuya-Yoshida (RKKY) interaction[3] and the Kondo effect in this compound. At low temperature the RKKY interaction, which couples the Ce $4f$ magnetic moments to each other, predominates and the compound shows antiferromagnetic order. The Ce magnetic moments are aligned in opposite directions in the neighboring (111) planes. The magnetic moment of this compound is strongly pressure dependent and might be suppressed at a critical pressure $P_C \approx 2.55$ GPa.[4] Through increasing the hydrostatic pressure, the Kondo state is stabilized and the antiferromagnetic state becomes unstable so that T_N decreases down to 0 K.[5] $CeIn_3$ shows superconductivity in a narrow region of pressure and temperature values below 0.2 K and around $P_C \approx 2.5-2.7$ GPa in the vicinity of specific quantum critical point.[2] Superconductivity appears near the magnetic ordering. This indicates that the magnetic interaction, which is maximum near P_C, is somehow effective on superconductivity.

The properties of $CeIn_3$ have been extensively studied by several authors.[1–15] Here, we have focused on the numerical analysis for the critical pressure of this compound. In this work we have used the first-principles calculations based on density-functional theory (DFT) and employed the WIEN2K package[16] to investigate the structural and electronic properties of $CeIn_3$. The more advanced methods of augmented plane waves plus local orbital (APW+lo) (Refs. 17 and 18) were used to linearize the energies. In addition to the standard Perdew-Burke-Ernzerhof (PBE) generalized gradient approximation (GGA) (Ref. 19) calculations, we have used here the nonempirical GGA as proposed recently by Wu and Cohen (WC).[20] The new GGA (WC) exchange-energy functional, which is used in combination with the PBE correlation-energy functional, has shown improvements upon the widely used GGA (PBE) results. Practically, the structural parameters are on average closer to the experiment.[21] We report the electronic calculations within the WC-GGA functional for this compound. The goal of this work is to investigate the behavior of Ce magnetic moment under pressure and to calculate the critical pressure at which magnetic moment is suppressed. We also look for the effect of pressure on In electric field gradient (EFG).

The paper is organized as follows. A brief description of the calculation method is given in Sec. II. Section III contains the results and discussion of the equation of state (EOS) and electronic structure for $CeIn_3$ compound. Section IV gives a brief summary and conclusion of this work.

II. NUMERICAL IMPLEMENTATION

$CeIn_3$ crystallizes in the space group of $Pm\bar{3}m$ with cubic structure of $AuCu_3$ prototype. This structure is stable under pressure up to 10 GPa.[8] The point group of Ce and In atoms are the cubic m-$3m$ and noncubic $4/mmm$, respectively. The lattice parameter of $CeIn_3$ is 4.689 Å. Ce atoms are located at the corners and In atoms are located at the face-centered positions of a cubic unit cell.

We performed the calculations using the full-potential APW+lo method. This is a highly accurate technique based on DFT,[22] implemented in the WIEN2K code. A fully relativistic description for the core states and a scalar-relativistic description for the valence states were used. For structural and electronic properties, we have calculated the exchange-correlation potential using two generalized gradient approximations, the PBE-GGA and the newly implemented WC-GGA routine.[20]

The full-potential linear augmented plane-wave (FP-LAPW) method divides space into an interstitial region (IR) and nonoverlapping muffin-tin (MT) spheres centered at the atomic sites. In the IR, the basis consists of the plane waves while inside the MT spheres, the basis is described by radial solutions of the one-particle Schrödinger equation (at fixed energy) and their energy derivatives multiplied by spherical harmonics. In order to achieve a convergence for eigenvalues the wave function in the interstitial region were expanded in-plane waves with a cutoff at $K_{max}=7.0/R_{MT}$. R_{MT} denotes the smallest atomic sphere radius and K_{max} gives the magnitude of the largest K vector in the plane-wave expansion. The muffin-tin radii (R_{MT}) were taken to be 2.3 Bohr (1 Bohr =0.529177 Å), for both In and Ce atoms. The ($5s^2$, $5p^6$, $4f^1$, $5d^1$, and $6s^2$) atomic states of Ce and ($4p^6$, $4d^{10}$, $5s^2$, and $5p^1$) states of In were considered as valence states. The maximum quantum number l for atomic wave functions inside the sphere was confined to $l_{max}=10$. The charge density was Fourier expanded up to $G_{max}=14$ $Ry^{1/2}$. A mesh of 72 k points was chosen in the irreducible wedge of the Brillouin zone, which corresponds to the grids of $12\times12\times12$ in the scheme of Monkhorst-Pack. After adding spin-orbit coupling (SOC), a mesh of 184 k point in the irreducible wedge of the Brillouin zone was generated. The SOC Hamiltonian was diagonalized in the space of scalar-relativistic eigenstates using a second-variational procedure. We also imposed (111) direction on the Ce magnetic moments. A $2\times2\times2$ antiferromagnetic super cell was thus obtained. Then the total energy for different volumes has been fitted to the Birch-Murnaghan EOS.[23]

III. RESULTS AND DISCUSSION

A. Static equation of state and bulk modulus

The total energy for seven different volumes of antiferromagnetic $CeIn_3$ was calculated both in the presence of spin-orbit coupling (AFM+SOC) and in the absence of spin-orbit coupling (AFM) using PBE-GGA and WC-GGA for exchange-correlation functional. WC-GGA has been recently formulated by Wu and Cohen. It is based on a diffuse radial cutoff for exchange hole in real space and the analytical gradient expansion of the exchange energy for small gradients.[20] It shows improvement for lattice constant, crystal structure, and bulk modulus over the common PBE-GGA method.[20]

Oomi *et al.*[8] measured V/V_0 as a function of pressure up to 10 GPa in which V_0 is the standard volume at $P=0$. In Fig. 1, the calculated pressures through equation of states using PBE-GGA and WC-GGA in the range of −5 to +22 GPa are compared with their experimental data. In this figure, V/V_0 is plotted for both experimental V_0 and computed V_0, which is

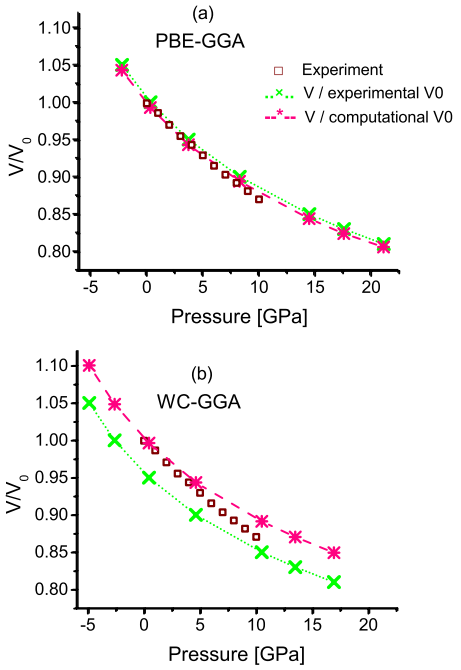

FIG. 1. (Color online) Comparison between V/V_0 as a function of computed pressures from Birch-Murnaghan equation of state (AFM+SOC). Dotted (green) lines indicate experimental V_0 and dashed (pink) lines are computed V_0 for the minimum of energy using (a) PBE-GGA functional and (b) WC-GGA functional with experimental results of Oomi *et al.* (Ref. 8) for $CeIn_3$ compound.

obtained from the lattice constant of minimum energy in Birch-Murnaghan equation. According to this figure, PBE results show a better agreement with experimental data over WC. It is noticeable that the plot without SO coupling (not shown in Fig. 1) traces out plot with SO coupling. It can be seen in this figure that the differences between theory and experiment are larger at high pressures. These differences are related to the different high- and low-pressure behaviors of $CeIn_3$. It is known that the systematic deviations from the simple equation of state can be used to find the phase transition.[24] The experimental measurements show that $AuCu_3$ structure of this compound is stable under pressures up to 10 GPa (Ref. 8) so that the crystal structure transition is not responsible for this inconsistency. As we will discuss in the next section, the magnetic moment of Ce is suppressed under pressure and the electronic transition from antiferromagnetic to nonmagnetic phase may cause a change through compression process.

Furthermore, through the Birch-Murnaghan fit one can obtain the equilibrium lattice constant. The corresponding equilibrium lattice parameters, bulk modulus, and derivative of bulk modulus are compared with the experimental results in Table I. It is obvious from this table that for $CeIn_3$ compound the equilibrium lattice constant calculated by PBE is closer to the experimental data than that of WC. But for bulk modulus, $B=-VdP/dV$, WC results are in better agreement with experiment over PBE. It means that the tangent to the volume-pressure diagram at zero pressure which shows bulk modulus is in good agreement with related experimental data.

TABLE I. The equilibrium lattice constant a_{min} in Angstrom, bulk modulus B_0 in GPa, and derivative of bulk modulus B_0' of $CeIn_3$ in comparison with experimental and other theoretical data.

	PBE-GGA		WC-GGA		
	AFM	AFM+SOC	AFM	AFM+SOC	Expt.
a_{min}	4.691	4.702	4.610	4.616	4.689[a]
B_0	58.85	55.22	68.45	66.46	67[b]
B_0'	4.73	5.30	4.94	5.36	

[a]Reference 7.
[b]Reference 8.

This agreement appears despite the fact that the calculated lattice constant using WC shows a deviation from experiment. It is also observed that including the spin-orbit coupling does not amend the structural results.

B. Electronic structure

Next we turn our attention to the total and partial DOS both in the absence of spin-orbit coupling (AFM) and in the presence of spin-orbit coupling (AFM+SOC). The calculations were performed including SOC for Ce and In electrons. The PBE-GGA and WC-GGA were used for exchange-correlation functional. In addition, we have considered the effect of pressures up to 22 GPa for all phases.

In Fig. 2 total density of states in $CeIn_3$ are shown for two pressure values $P=0.0$ and 17.0 GPa, calculated through the WC-GGA. All considered valence states are present in this figure except the In $4p$ states which lie at the deeper energy about −5 Ry and Ce $5s$ states which have a very small density of states at the energy of approximately −0.5 Ry. Ce $5p$ and In $4d$ states remain atomiclike located at 1.29 and 1.04 Ry below Fermi level, respectively. Other states, Ce ($4f$, $5d$, and $6s$) and In ($5s$ and $5p$) are located around Fermi level. The SOC not only influences the semi core states of Ce $5p$ and In $4d$ but also changes the density of states at the Fermi level [DOS (E_F)]. On the other hand, the approximation which is used for exchange-correlation functional can affect DOS (E_F). EFG is very sensitive to the value of the DOS (E_F) so that the SOC and the specific type of functional approximation can influence EFG. We will bring up EFG issue more in depth, in the next section. In addition, in both approximations and for all pressures studied here f and d states of Ce and p orbital of In have more contributions to DOS(E_F), in a descending order (for PBE-GGA see Fig. 2 of Ref. 15).

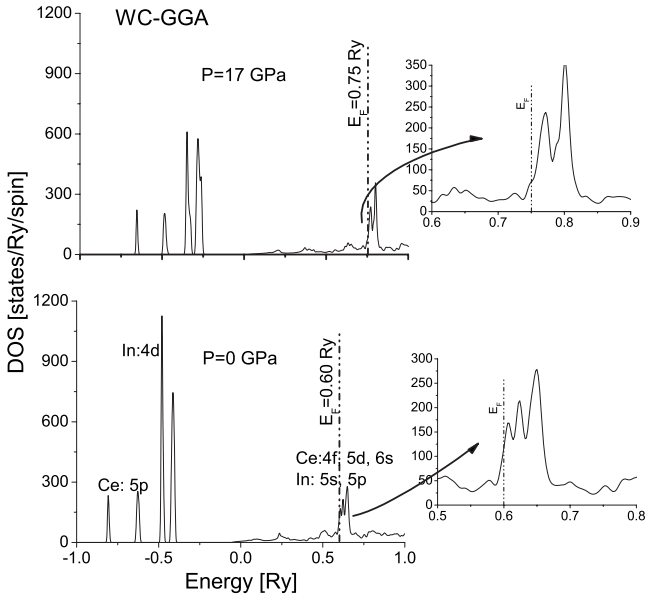

FIG. 2. Total density of states in $CeIn_3$ for two different pressures, obtained by FP-APW method using WC-GGA, in the presence of spin-orbit coupling. The insets show a magnified picture of DOS around Fermi level.

One can see in Fig. 2 that all states considered as valence states move into higher energies under pressure. Ce $5p$ state and In $4d$ state which are core states also move into higher energies under pressure while keeping their atomiclike nature. We note that during the displacement of Fermi level and valence states into higher energies under pressure, the distance of Ce $5p$ states from Fermi level remains constant while the distance of In $4d$ states from this level begins to increase. We have not observed any drastic changes in DOS under pressure. The compound does not show any structural transitions under pressure up to the maximum pressure studied (i.e., 22 GPa). We note that available experimental results for $AuCu_3$ structure of this compound show stability up to 10 GPa.[8]

The $CeIn_3$ is an antiferromagnetic compound. Lawrence and Shapiro[6] reported a value of $0.65 \pm 0.1 \mu_B$ for its magnetic moment from neutron-diffraction experiment at $T=5$ K while Benoit *et al.*[7] achieved a value of $0.48 \pm 0.08 \mu_B$ from neutron-diffraction study at $T=3$ K. In our recent work,[15] using density-functional theory, we found that the spin magnetic moment for the equilibrium lattice constant at the Ce atom through PBE and PBE+SOC are 0.658 and $0.715 \mu_B$, respectively. Again these amount to $0.521 \mu_B$ using WC and $0.564 \mu_B$ using WC+SOC at $T=0$ K. We have also included the orbital contribution to magnetic moment. Orbital magnetic moment is calculated to be −0.545 using PBE+SOC and $-0.452 \mu_B$ through WC+SOC, with its direction opposite to the spin magnetic moment. Lalić *et al.*[10] have found a value of $0.708 \mu_B$ for spin magnetic moment and $-0.531 \mu_B$ for orbital magnetic moment by using FP-LAPW method and SOC at $T=0$ K. So the total magnetic-moment values on Ce amount to $0.170 \mu_B$ using PBE+SOC and $0.112 \mu_B$ through WC+SOC, in our analyses, respec-

TABLE II. The contributions of s, p, d, and f shells in spin (SPI) and orbital (ORB) magnetic moments of Ce in $CeIn_3$ compound in the units of μ_B computed in the present work using the equilibrium of lattice constant.

	PBE-GGA AFM+SOC					WC-GGA AFM+SOC				
	s	p	d	f	Tot	s	p	d	f	Tot
SPI	0.003	0.006	0.062	0.644	0.715	0.002	0.005	0.048	0.509	0.564
ORB	0.000	0.000	−0.005	−0.540	−0.545	0.000	0.000	−0.003	−0.449	−0.452
SPI+ORB	0.003	0.006	0.057	0.104	0.170	0.002	0.005	0.045	0.060	0.112
SPI[a]	0.003	0.005	0.061	0.639	0.708					
ORB[a]				−0.528	−0.531					
SPI+ORB				0.111	0.177					

[a]Reference 10.

tively. Our result for PBE is close to the Lalić result of $0.177\mu_B$. However, there is a rather poor agreement between simulation and experimental results. It can be seen that making use of WC-GGA does not remove this disagreement. Our findings point out that p, d, and f states contribute to the magnetic moment of $CeIn_3$ with Ce f states being the largest component at all pressure from −5 to 22 GPa. These values are reported in Table II for zero pressure (i.e., for equilibrium lattice constant). It is also observed that x, y, and z components of Ce magnetic moment have equal values. Moreover the spin and orbital parts of magnetic moment at Ce sites are in opposite directions except for p orbital. No net magnetic moment is found at the In position, whereas small values of 0.002 and $0.003\mu_B$ are obtained using PBE+SOC and WC+SOC, respectively. The In $5p$ contribution ($0.001\mu_B$) is dominant at all pressures studied.

$CeIn_3$ shows an antiferromagnetic order below $T_N=10$ K. With pressure, the magnetic moment of Ce is suppressed at a critical pressure P_C. It is known that, a pressure-induced superconductivity appears in the vicinity of a critical pressure where the Néel temperature is shifted down to zero.[2] The behavior of Ce magnetic moment attracted much attention via de Haas-van Alphen experiments under pressures up to 2.7 GPa.[11] They found a change in the shape of a spherical Fermi surface with humps along (111) at $P_C=2.5$ GPa and $T=108$ mK. In Ref. 12 Settai *et al.* have found $P_C=2.72$ GPa using the same method along (110). Grosche *et al.*[4] studied $CeIn_3$ in a series of resistivity measurements at high pressures up to 3.2 GPa and down to temperatures in the mK region. They found P_C to be 2.55 GPa. We have investigated the behavior of both spin and orbital magnetic moment of Ce under pressure. As Fig. 3(a) shows, the spin magnetic moment of Ce is strongly pressure dependent and decreases with increasing the pressure. The results show an almost linear fall of spin magnetic moments of Ce by increasing the pressure. This again confirms the result of Ref. 15. We found there an almost linear dependence of Ce magnetic moment on Ce $4f$ density of states at Fermi level for certain range of parameters. To obtain the critical pressure, we have plotted the total magnetic moment of Ce as a function of pressure in Fig. 3(b). It shows that using PBE-GGA the total magnetic moment is suppressed at $P_C=16$ GPa. This is not in good agreement with experimental data. So we tried WC-GGA and obtained a critical pressure of 9 GPa which is in better agreement with experiment. Since Ce magnetic moment almost completely originates from f shell, we investigated the effect of pressure on the density of states of Ce $4f$. The $4f$-DOS of the AFM+SOC phase at two pressures are illustrated in Fig. 4. In this case one can see that by increasing pressure the f band broadens and simultaneously moves away from Fermi level into the conduction band. As f electrons become more and more itinerant, the magnetic moment decreases.

C. Electric field gradient

There is an electric field gradient at the In sites due to the noncubic point symmetry. The EFG is the gradient of the

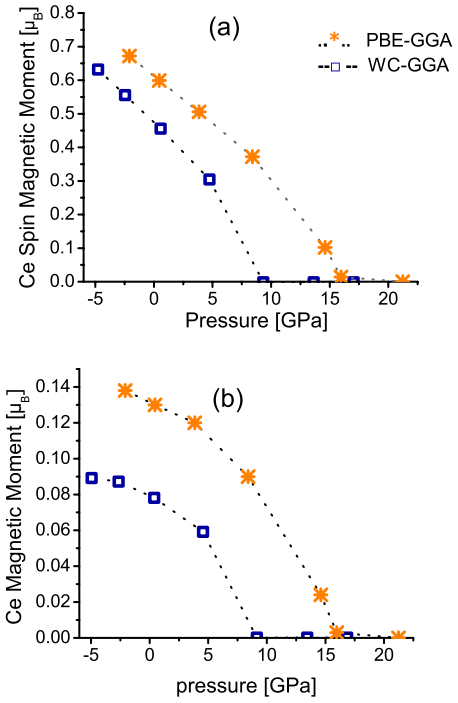

FIG. 3. (Color online) (a) Spin magnetic moment and (b) total magnetic moment of Ce in $CeIn_3$ compound under pressure.

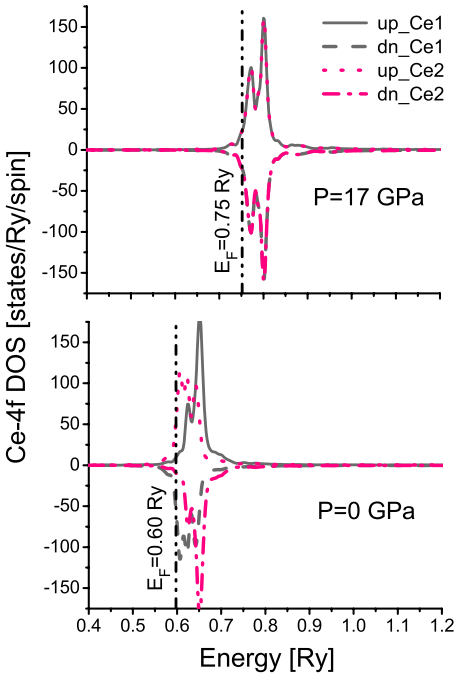

FIG. 4. (Color online) Spin-up and spin-down Ce 4*f*-DOS in $CeIn_3$ at two pressures evaluated by WC-GGA functional. Fermi levels are shown as solid vertical lines.

electrostatic field at the nuclear position. It is dominantly generated by valence electrons inside the atomic sphere. The EFG is a traceless symmetric tensor of rank 2, defined as the second derivative of electrostatic potential of electron distribution with respect to special coordinates evaluated at the position of the nucleus ($\vec{r}=\vec{0}$),[25]

$$V_{ij} = \frac{\partial^2 V(0)}{\partial x_i \, \partial x_j}. \tag{1}$$

One should provide five independent quantities in order to determine the tensor unambiguously. The EFG tensor has only two independent components in the principal axes system; the main component of the EFG, V_{zz} and the asymmetry parameter $\eta=(V_{xx}-V_{yy})/V_{zz}$. These two quantities can usually be determined from experiment. V_{zz} can be obtained from the charge density $\rho(\vec{r})$,

$$V_{zz} = \int \rho(r) \frac{2P_2(\cos\vartheta)}{r^3} dr. \tag{2}$$

In the LAPW method, $\rho(\vec{r})$ is expressed by lattice harmonics (i.e., under an LM form),

$$\rho_{LM}(r) = \sum_{E<E_F} \sum_{lm} \sum l'm' R_{lm}(r) R_{l'm'}(r) G_{Lll'}^{Mmm'}. \tag{3}$$

The R_{lm}'s are radial functions with angular momentum l or l' and the G's are the so-called Gaunt numbers (an integral over a product of spherical harmonics). The contribution of the electrons inside the muffin-tin sphere is called the valence EFG, which here is denoted by V_{zz}^{val}. The contributions of the electrons at the surface and outside of the spheres are called lattice EFG, denoted by V_{zz}^{lat}.

In our study, due to the presence of a threefold symmetry axis, the asymmetry parameter η is zero. The main component of electric field gradient has been measured for $CeIn_3$ by various methods. Employing the time differential perturbed angular correlation technique for measuring the electric field gradient at In site and at temperature range of 4.2–10 K showed a $V_{zz}=4.07\times10^{21}$ V/m^2.[5] The electric field gradient at In site is also measured using ^{115}In nuclear quadrupole resonance at 4.2 K and yields $V_{zz}=11\times10^{21}$ V/m^2.[9] We have also calculated the electric field gradient V_{zz} and its respective valence V_{zz}^{val} and lattice V_{zz}^{lat} components with and without spin-orbit coupling by PBE-GGA and WC-GGA. The calculated EFGs at In sites for the equilibrium lattice constants are summarized and compared with the reported values in Table III. As is evident in this table the results of PBE-GGA are closer to experiment than WC-GGA, especially, after SOC. Before applying SOC, to our model $CeIn_3$

TABLE III. The main component of electric field gradients V_{zz} its decomposition to valence V_{zz}^{val} and lattice V_{zz}^{lat} components in the units of 10^{21} V/m^2 at Ce and In sites of $CeIn_3$ in the present work using the equilibrium lattice constant. Comparisons with previous results and experimental data are also given. Experimental EFG at In site 11.6×10^{21} V/m^2 (Ref. 9).

	PBE-GGA						WC-GGA					
	AFM			AFM+SOC			AFM			AFM+SOC		
	V_{zz}	V_{zz}^{val}	V_{zz}^{lat}	V_{zz}	V_{zz}^{val}	V_{zz}^{lat}	V_{zz}	V_{zz}^{val}	V_{zz}^{lat}	V_{zz}	V_{zz}^{val}	V_{zz}^{lat}
In[a]	12.624	12.675	−0.051	12.446	12.496	−0.05	13.356	13.417	−0.061	13.152	13.208	−0.056
Ce				0.055	0.049	0.006				0.049	0.047	0.002
In[b]	13.027	13.032	−0.005	12.957	12.961	−0.004						
Ce	0.089	0.086	−0.003	0.029	0.040	−0.011						
In[c]				12.490	12.540	−0.050						
Ce												

[a]Present work.
[b]Reference 13.
[c]Reference 10.

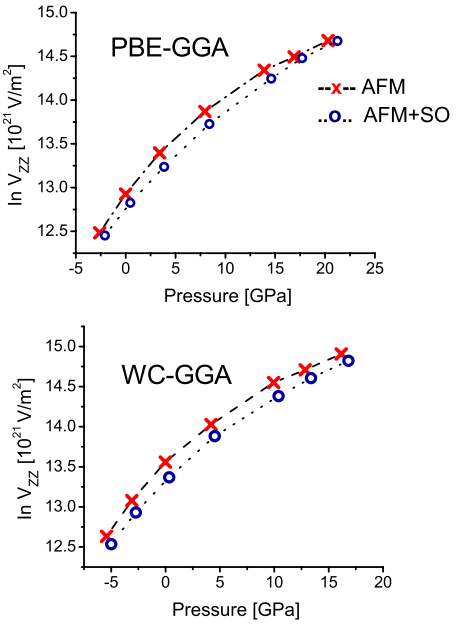

FIG. 5. (Color online) The calculated electric field gradient under pressure at In site, without and with spin-orbit coupling using PBE and WC approximations.

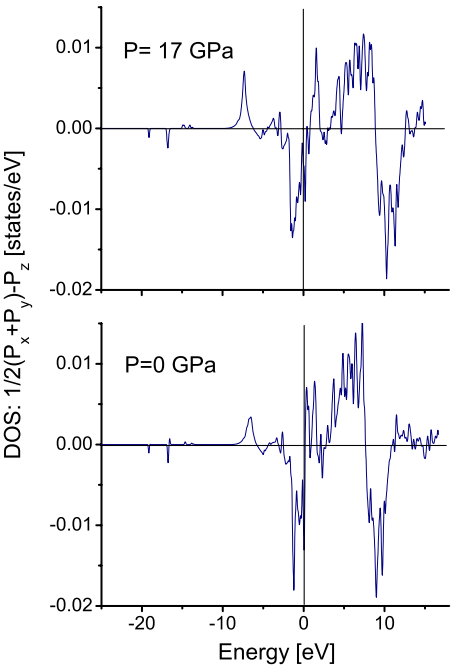

FIG. 6. (Color online) The contribution of $\frac{1}{2}(p_x+p_y)-p_z$ in the DOS at two different pressures.

compound, due to the noncubic structure only In nuclei exhibit the electric quadrupole interaction but after incorporating the SOC effect, we also observe a small EFG at Ce site. It seems that spin-orbit interaction reduces the symmetry around the Ce position.

We have also investigated the EFG behavior under pressure. The EFG at Ce sites with a cubic environment without SO coupling is zero up to 22 GPa. While at In sites it increases for all foregoing approximation in a bowing shape with increasing the pressure. (See Fig. 5.) By inspecting the partial DOS, one can easily understand the reason for increasing the EFG with increasing pressure. The EFG in this compound originates from In $5p$ shells.[15] A measure for the nonspherical charge distribution based on p charges inside the muffin-tin sphere can be written as[26]

$$\Delta n_p = \frac{1}{2}(n_{p_x} + n_{p_y}) - n_{p_z}. \tag{4}$$

We calculated the term $\Delta p = \frac{1}{2}(p_x+p_y)-p_z$ over a wide pressure range, where p_i is the partial DOS of p orbital in i direction. In Fig. 6, Δp is shown for two typical pressures. The dominant part of nonsphericity in the charge distribution increases with pressure from $\Delta n_p = -0.009$ at $P=0$ GPa to -0.013 at $P=17$ GPa. Therefore, the resultant In EFG increases with pressure too. The dominance of the p_z below the Fermi energy is noticeable and this leads to the negative value of Δn_p.

IV. CONCLUSIONS

We have investigated the effect of pressure on magnetic moment of antiferromagnetic $CeIn_3$ using recently proposed Wu-Cohen generalized gradient approximation. Spin-orbit interaction has been included in the calculations. For certain values of pressure, result shows a perfect antiferromagnetic ordering of Ce originating mostly from $4f$ states. The pressure affects the behavior of electrons and changes them from bound to itinerant and suppresses the magnetic moment at a critical value, P_C. P_C is calculated to be 16 GPa by PBE-GGA. Implementation of WC-GGA improves P_C to 9 GPa. WC-GGA approach also amends the results of calculated bulk modulus. While WC authors expect an improvement in the calculation of structural parameters over the standard PBE, in our study the values of lattice constant and EFGs are not improved. We have also investigated the variations in EFGs and their valence contributions at both Ce and In sites under pressure. The EFG at In site increases bowing with increasing the pressure. Since EFG originates from nonsphericity of nuclear charge distribution, the pressure reduces the symmetry at In site. Furthermore, by applying SO coupling, we observe a small EFG at Ce site.

*Corresponding author; ilkhaniirn@shahryariau.ac.ir

[1] N. V. Chandra Shekar, M. Rajagopalan, J. F. Meng, D. A. Polvani, and J. V. Badding, J. Alloys Compd. **388**, 215 (2005).
[2] N. D. Mathur, F. M. Grosche, S. R. Julian, I. R. Walker, D. M. Freye, R. K. W. Haselwimmer, and G. G. Lonzarich, Nature (London) **394**, 39 (1998).
[3] M. A. Ruderman and C. Kittle, Phys. Rev. **96**, 99 (1954); T. Kasuya, Prog. Theor. Phys. **16**, 45 (1956); K. Yosida, Phys. Rev. **106**, 893 (1957).
[4] F. M. Grosche, I. R. Walker, S. R. Julian, N. D. Mathur, D. M. Freye, M. J. Steiner, and G. G. Lonzarich, J. Phys.: Condens. Matter **13**, 2845 (2001).
[5] A. W. Carbonari, J. Mestnik-Filho, R. N. Saxena, and H. Saitovitch, Hyperfine Interact. **133**, 77 (2001).
[6] J. M. Lawrence and S. M. Shapiro, Phys. Rev. B **22**, 4379 (1980).
[7] A. Benoit, J. K. Boucherle, P. Convert, J. Flouquet, J. Palleau, and J. Schweizer, Solid State Commun. **34**, 293 (1980).
[8] G. Oomi, T. Kagayama, and J. Sakurai, J. Mater. Process. Technol. **85**, 220 (1999).
[9] Y. Kohori, Y. Inoue, T. Kohara, G. Tomka, and P. C. Riedi, Physica B **259-261**, 103 (1999).
[10] M. V. Lalić, J. Mestnik-Filho, A. W. Carbonari, R. N. Saxena, and H. Haas, Phys. Rev. B **65**, 054405 (2001).
[11] R. Settai, T. Kubo, H. Shishido, T. C. Kobayashi, and Y. Onuki, J. Magn. Magn. Mater. **272-276**, 223 (2004).
[12] R. Settai, T. Kubo, H. Shishido, T. C. Kobayashi, and Y. Onuki, Physica B **359-361**, 317 (2005).
[13] S. Jalali Asadabadi, Phys. Rev. B **75**, 205130 (2007).
[14] C. I. Lee, K. E. Lee, Y. Y. Song, H. J. Im, S. Kimura, and Y. S. Kwon, Infrared Phys. Technol. **51**, 488 (2008).
[15] M. Ilkhani, M. R. Abolhassani, and M. Aslaninejad, Eur. Phys. J. B **65**, 21 (2008).
[16] P. Blaha, K. Schwarz, G. K. H. Madsen, D. Kvasnicka, and J. Luitz, *WIEN2K, An Augmented plane Wave + Local Orbitals Program for Calculation Crystal Properties*, edited by Karlheinz Schwarz (Techn. Universität Wien, Austria, 1999).
[17] E. Sjöstedt, L. Nordström, and D. J. Singh, Solid State Commun. **114**, 15 (2000).
[18] G. K. H. Madsen, P. Blaha, K. Schwarz, E. Sjöstedt, and L. Nordström, Phys. Rev. B **64**, 195134 (2001).
[19] J. P. Perdew, K. Burke, and M. Ernzerhof, Phys. Rev. Lett. **77**, 3865 (1996).
[20] Z. Wu and R. E. Cohen, Phys. Rev. B **73**, 235116 (2006).
[21] F. Tran, R. Laskowski, P. Blaha, and K. Schwarz, Phys. Rev. B **75**, 115131 (2007).
[22] P. Hohenberg and W. Kohn, Phys. Rev. **136**, B864 (1964); W. Kohn and L. J. Sham, Phys. Rev. **140**, A1133 (1965).
[23] F. D. Murnaghan, Proc. Natl. Acad. Sci. U.S.A. **30**, 244 (1944).
[24] R. E. Cohn, O. Gülseren, and R. J. Hemley, Am. Mineral. **85**, 338 (2000).
[25] K. Koch and S. Cottenier, Analysis of an EFG: the EFG switch in LAPW2, available from: http://www.wien2k.at/reg_user/faq (2006).
[26] P. Blaha, K. Schwarz, and P. Herzig, Phys. Rev. Lett. **54**, 1192 (1985).